RESEARCH ARTICLE

Interfacial microenvironments enable abiotic ribonucleoside formation in micro- and nanoscale compartments

Qiang Liu, Xia Zhao, Jae Kyoo Lee, and Richard N. Zare Authors Info & Affiliations

Contributed by Richard N. Zare; received July 11, 2026; accepted September 7, 2026; reviewed by Jeffrey E. Dick and Hailin Wang

October 12, 2026 | 123 (42) e2624803123 | https://doi.org/10.1073/pnas.2624803123

PDF EPUB

Significance

The origin of ribonucleosides, essential building blocks of RNA, remains a major unresolved problem in prebiotic chemistry because their abiotic formation is inefficient and their stability is limited under plausible early-Earth conditions. We show that interfacial environments within compartmentalized micro- and nanoscale systems promote ribonucleoside formation without enzymatic catalysis across a diverse range of physicochemical settings, including micro/nanobubbles, lipid vesicles, and microemulsions. Reaction efficiency and product stability depend strongly on interfacial architecture, compartment size, and coupled gas–liquid and liquid–liquid interfaces. These findings identify compartmentalized interfacial systems as a general physical framework for ribonucleoside emergence and suggest that ubiquitous heterogeneous interfaces on early Earth could have facilitated key steps toward the origin of RNA-based life.

Abstract

The abiotic emergence of ribonucleosides remains a central challenge in origin-of-life research because ribonucleosides form inefficiently and are often unstable under prebiotically plausible conditions. Here we show that interfacial microenvironments within aqueous micro- and nanoscale compartments containing D-ribose, phosphoric acid, and nucleobases promote ribonucleoside formation by creating reaction-permissive physicochemical conditions independent of the specific compartment type. Across a diverse range of compartmentalized systems, including gas–oil–water micro/nanobubbles, gas–water micro/nanobubbles, microscale lipid-bilayer vesicles, and oil–water emulsion systems, ribonucleosides form abiotically in the absence of enzymatic catalysis. Under selected interfacial conditions, multiple ribonucleosides,

including cytidine, are generated without added catalysts. Comparison among these systems reveals that interfacial architecture and coupled physicochemical properties strongly influence both reaction efficiency and product stability. CO_2-based micro/nanobubbles support sustained cytidine accumulation, highlighting the importance of coupled gas–liquid and liquid–liquid interfaces. Ribonucleoside synthesis also depends on compartment size, whereas variations in oil content within micro/nanobubbles selectively modulate inosine formation, underscoring the sensitivity of nucleoside chemistry to interfacial properties. These findings identify interfacial microenvironments within micro- and nanoscale compartments as a general physical framework for ribonucleoside emergence and suggest that ubiquitous compartmentalized interfaces on early Earth could have provided robust settings for prebiotic ribonucleoside chemistry.

Sign up for PNAS alerts.

Get alerts for new articles, or get an alert when an article is cited.

LEARN MORE

The origin of life is constrained not only by chemical feasibility, but also by the physical environment in which chemistry occurs (1, 2). Although prebiotic research has traditionally focused on reaction pathways and catalytic optimization (3), comparatively little attention has been paid to how the spatial organization of reactions at the micro- and nanoscale influences chemical reactivity. On early Earth, interfaces were likely ubiquitous, emerging naturally from gas–water, liquid–water, and solid–water systems (4). This ubiquity was further reinforced by a CO_2-rich and oxygen-poor atmosphere (5, 6). Such interfaces could create physically structured reaction spaces capable of concentrating molecules, maintaining localized physicochemical conditions, and promoting reactions that would otherwise be inefficient or unfavorable in bulk solutions. This process could be further aided by wet–dry cycles that promote biomolecular polymerization (7). Understanding how such interfacial microenvironments actively regulate chemical processes is therefore essential to reconstructing plausible routes toward life's molecular building blocks (2).

Against this physical backdrop, the abiotic formation of ribonucleosides remains a central challenge in origin-of-life research, largely owing to low reaction efficiency and poor product stability under prebiotically plausible conditions. Here, we explore whether micro- and nanoscale compartments could provide interfacial microenvironments that enable ribonucleoside emergence without enzymatic catalysis. Specifically, we examine three different compartment architectures: micro/nanobubbles, microscale lipid-bilayer vesicles, and oil–water emulsion systems. Within the bubble platform, gas–water (G/W) and gas–oil–water (G/O/W) configurations were compared to assess the role of coupled gas–liquid and liquid–liquid interfaces.

By comparing these compartment architectures, we ask whether ribonucleoside emergence depends on a specific compartment type or on shared interfacial features of micro- and nanoscale reaction environments. We further examine how gas composition, oil–water interfaces, addition of a mineral, and compartment size modulate reaction permissiveness across these systems. This comparative study allows us to test interfacial microenvironments as a physical framework for abiotic ribonucleoside formation under ambient conditions relevant to prebiotic chemistry. By placing chemical reactivity in the context of micro- and nanoscale physical environments, this study provides a framework for considering how ubiquitous interfacial compartments could have supported the formation of RNA building blocks in prebiotic chemistry.

Methods

Micro- and nanoscale bubbles containing coupled gas–oil–water (G/O/W) interfaces were generated using three independent physical approaches: sonication (8), double-syringe mixing (9), and air-stone aeration (10) (Fig. 1*A*). The resulting G/O/W micro/nanobubbles were designed as one of three compartment architectures examined in this study, together with microscale lipid-bilayer vesicles and oil–water emulsion systems (Fig. 1 *B–D*). These systems provide distinct interfacial environments in which ribose, phosphate, and nucleobases can be organized within confined aqueous regions. The overall reaction scheme for ribonucleoside emergence from D-ribose, phosphoric acid, and nucleobases is illustrated in Fig. 1*E*.

Fig. 1.

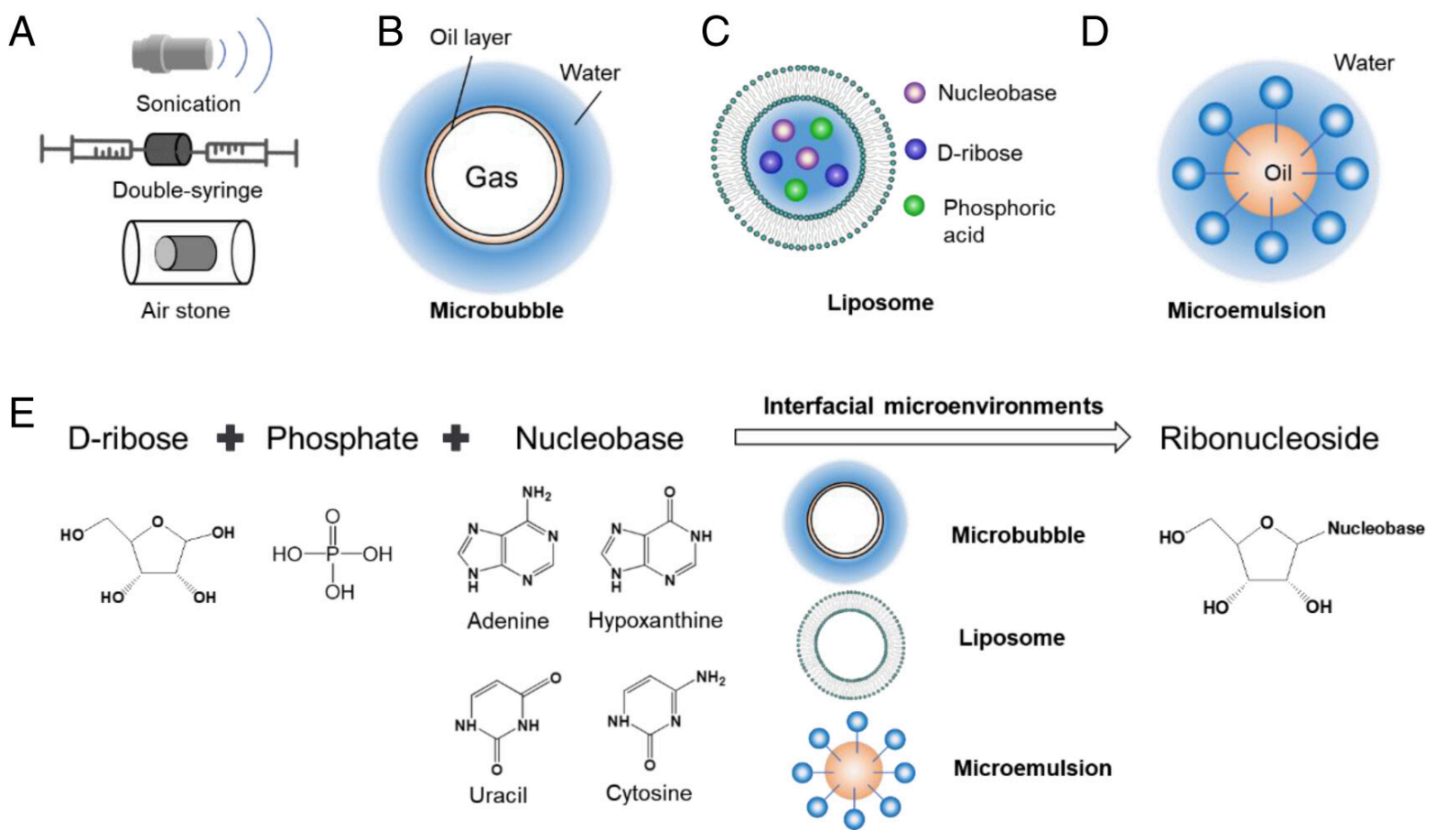

Interfacial microenvironments in micro- and nanoscale compartments investigated in this study. (A) Methods used to generate micro- and nanobubble compartments, including sonication, double-syringe mixing, and air-stone aeration. (B) Structure of gas–oil–water (G/O/W) micro/nanobubbles showing coupled gas–liquid and liquid–liquid interfaces forming confined aqueous interfacial microenvironments. (C) Micron-scale lipid-bilayer vesicles (liposomes) loaded with D-ribose, nucleobases, and phosphoric acid, forming membrane-bounded aqueous compartments. (D) Oil–water microemulsions (O/W MEs) showing nanoscale oil–water interfacial compartments. (E) Schematic representation of ribonucleoside formation from D-ribose, phosphoric acid, and nucleobases within compartmentalized interfacial microenvironments. These compartmentalized systems provide interfacial microenvironments that differ from bulk aqueous solutions and are used to evaluate ribonucleoside formation under confined conditions.

Rhodamine B staining showed fluorescence enrichment at the G/O/W boundary, consistent with local interfacial accumulation within the bubble compartment (*SI Appendix*, Fig. S1*A*). Separately, dynamic light scattering and zeta-potential measurements revealed a negative surface potential (−35.4 mV), supporting the colloidal stability of the G/O/W micro/nanobubbles. Under these conditions, ribonucleosides were detected selectively in micro- and nanobubble systems by electrospray ionization mass spectrometry (ESI-MS) (Fig. 2 and *SI Appendix*, Fig. S2). In contrast, matched control experiments performed in the absence of micro/nanobubbles yielded only protonated nucleobase signals, with no detectable ribonucleosides. More detailed information about the preparation of micro- and nanoscale compartments and the characterization of reaction products is presented in Table 1.

Fig. 2.

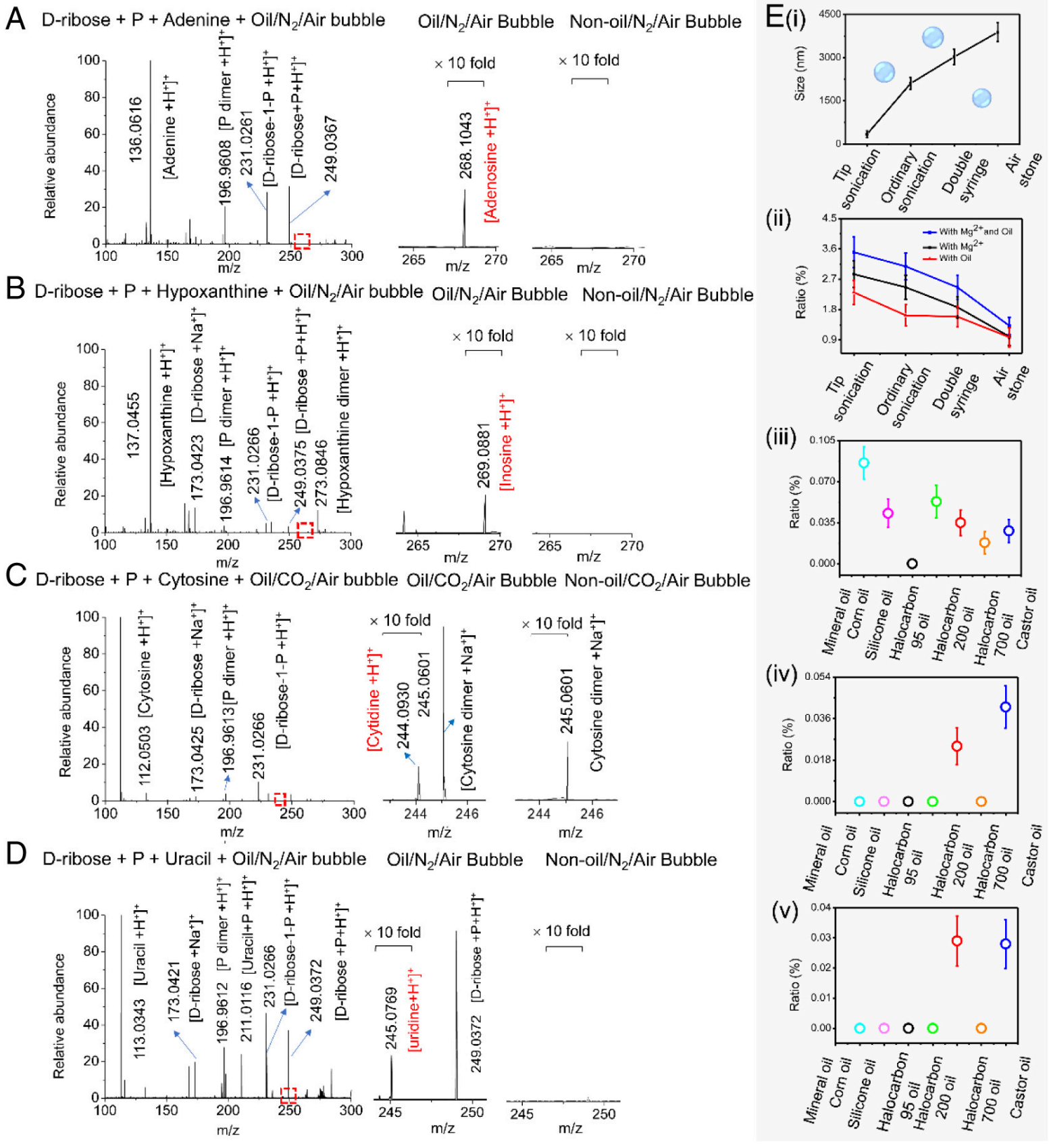

Ribonucleoside formation in gas–oil–water (G/O/W) micro- and nanobubble compartments. Representative ESI mass spectra showing protonated adenosine (A), inosine (B), cytidine (C), and uridine (D) formed in oil-containing micro- and nanobubble compartments, but not in gas–water (G/W) bubble controls lacking oil interfaces. Expanded views (Right panels) highlight nucleoside signals observed exclusively in G/O/W micro- and nanobubble compartments. (E) (i) Bubble sizes produced by different fabrication methods. (ii) MS-derived relative yield of uridine formation as a function of bubble size under different additive conditions. (iii–v) MS-derived relative yield of inosine formation in micro/nanobubbles generated by sonication, double-syringe mixing, and air-stone aeration using different oils.

Table 1.

Ribonucleoside formation across compartmentalized interfacial microenvironments under different gas and mineral conditions

				MS-derived relative yield of nucleo formation (%)*		
Micro/nanocompartment	**Dominant interface type**	**Gas**	**Mg^{2+}**	**Adenosine**	**Inosine**	**Uridine**
G/W micro/nanobubbles	Gas–water	N_2	+	~ 0.01	~ 0.03	~ 1.32
		Air	+	ND	ND	ND

EXPAND FOR MORE

* relative abundance.

ND, not detected under the examined conditions.

Results and Discussion

Gas–Oil–Water Interface-Enabled Ribonucleoside Formation in Micro- and Nanobubble Compartments.

As shown in Fig. 2*A*, reactions conducted in N_2–air micro/nanobubbles containing oil produced characteristic ion signals corresponding to protonated adenine [adenine $+H^+]^+$ (*m/z* 136.0616), phosphorylated ribose intermediates such as [D-ribose-1-phosphate + $H^+]^+$ (*m/z* 231.0261), and protonated adenosine [adenosine + $H^+]^+$ (*m/z* 268.1043). Comparable G/O/W-dependent signals were observed for inosine, cytidine, and uridine, with protonated inosine [inosine + $H^+]^+$ (*m/z* 269.0881), cytidine [cytidine + $H^+]^+$ (*m/z* 244.0930), and uridine [uridine + $H^+]^+$ (*m/z* 245.0769) detected under the corresponding conditions (Fig. 2 *B–D*). These nucleoside signals were absent in matched G/W or non-oil bubble controls.

Together, these results demonstrate that ribonucleosides form selectively within G/O/W micro- and nanobubble compartments, indicating that interface-associated microenvironments enable ribonucleoside formation in the absence of enzymatic catalysis. Because interfacial microenvironments are influenced by compartment dimensions, we further examined whether bubble size affects ribonucleoside formation. Bubble size was varied by changing fabrication methods and gas flow conditions (Fig. 2 *E*, *i*). Across all tested conditions, uridine formation increased with decreasing bubble size, irrespective of whether oil, Mg^{2+}, or both were present (Fig. 2 *E*, *ii*). Tip sonication, which generated smaller and more narrowly distributed bubbles, resulted in higher inosine formation compared with sonication (Fig. 2 *E*, *iii*), double-syringe mixing (Fig. 2 *E*, *iv*), and air-stone aeration (Fig. 2 *E*,*v*). These results suggest that smaller micro- and nanobubble compartments provide more favorable interfacial environments for ribonucleoside formation. As will be appreciated better in what follows, these results are consistent with previous studies showing that the strength of the electric field at the interface increases with curvature causing enhanced generation of H and OH radicals from the charge transfer reaction $H^+ + OH^- \rightarrow H + OH$ (11, 12). It is the presence of these radicals that drive the observed chemical transformations.

Gas-Dependent Modulation of Ribonucleoside Formation in Micro- and Nanobubble Microenvironments.

Micro/nanobubbles containing different gases were generated by the air-stone method to examine how gas composition modulates interfacial reactivity. Inosine formation was first examined under different gas and additive conditions. Inosine formation was observed in N_2 micro/nanobubbles in the presence of Mg^{2+}, halocarbon 200 oil, or their combination (Fig. 3*A*). In contrast, CO_2–air and air micro/nanobubbles required the combined presence of Mg^{2+} and oil to induce inosine formation and exhibited lower efficiencies. Notably, inosine was not detected in the absence of oil under any gas condition, underscoring the essential role of coupled gas–oil–water (G/O/W) interfaces.

Fig. 3.

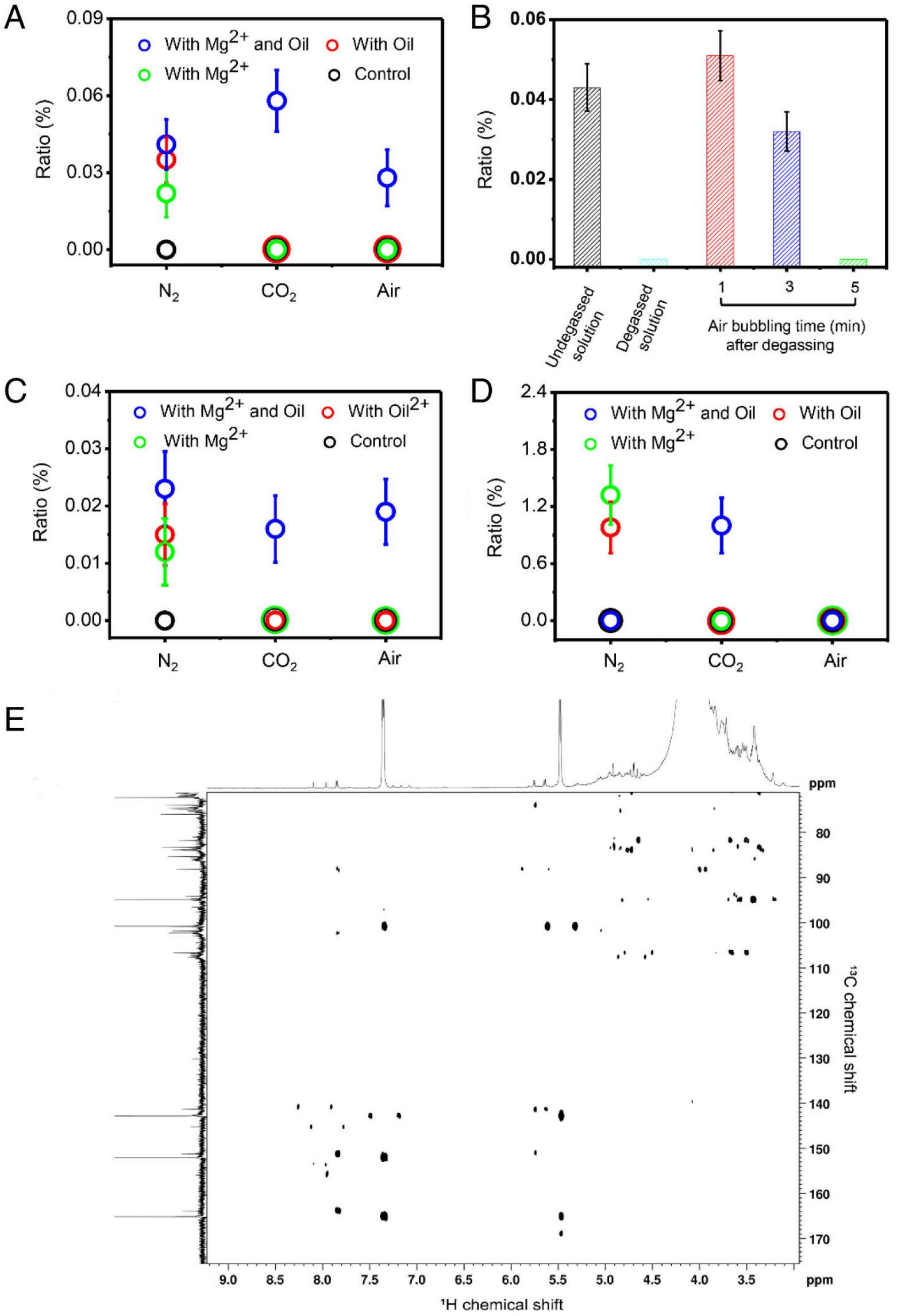

Gas-dependent ribonucleoside emergence in micro- and nanobubble compartments. (A and B) Inosine formation in micro/nanobubbles under (A) different gas and additive conditions and (B) controlled air reintroduction following degassing. Brief air reintroduction restores product accumulation; prolonged aeration reduces inosine accumulation. (C and D) Adenosine (C) and uridine (D) formation under different gas conditions, revealing nucleoside-specific gas dependencies. (E) HMBC spectrum showing key long-range correlations supporting N-glycosidic linkage and uracil moiety assignment.

To further probe the role of mixed-gas interfacial environments, degassing experiments were performed by purging the solution with N_2 for 30 min. Under these conditions, inosine signals were no longer detectable. Brief reintroduction of air (1 min) restored inosine formation, whereas prolonged aeration progressively suppressed activity, with no inosine detected after 5

min of air exposure (Fig. 3*B*). This nonmonotonic response indicates that inosine formation is favored under transient mixed-gas conditions rather than sustained aeration.

Adenosine and uridine exhibited distinct gas-dependent behaviors. Adenosine formation occurred predominantly in N_2–air micro/nanobubbles in the presence of Mg^{2+}, oil, or both, whereas N_2-only bubbles did not yield detectable adenosine. In contrast, uridine formation showed a different dependence, occurring in N_2–air micro/nanobubbles containing either Mg^{2+} or oil, but not both, whereas CO_2–air bubbles promoted uridine formation only when Mg^{2+} and oil were simultaneously present (Fig. 3 *C* and *D*). These nucleoside-specific responses indicate that gas composition and interfacial additives jointly regulate reaction outcomes.

Together, these results show that ribonucleoside formation is most efficient in micro/nanobubbles containing mixed N_2–air atmospheres compared with CO_2–air or air-only systems. Although these observations do not provide direct, interface-resolved evidence for the reaction locus, the strong dependences on gas composition, oil presence, and transient degassing–reaeration conditions are consistent with reactions occurring in interfacial microenvironments rather than in bulk aqueous solution. It might be wondered whether direct evidence exists that reactions occur at the interface. For reactions whose partners occupy different phases, the interface assignment is essentially unavoidable and is supported by single-droplet kinetics. For ordinary reactions with both reactants dissolved in the aqueous phase, most evidence remains circumstantial. Future studies using surface-sensitive spectroscopic approaches will be valuable for directly visualizing the interfacial localization of reaction intermediates and products. In such coupled G/O/W micro- and nanobubble systems, selective reactant enrichment and perturbed interfacial water structures could give rise to physicochemical conditions distinct from the bulk phase, potentially involving localized electric fields or reactive species (13–15). The enhanced reactivity observed under mixed N_2–air conditions may also be relevant to atmospheres with reduced O_2 levels, such as those proposed for early Earth (16).

Structural Confirmation of Uridine by Multidimensional NMR Spectroscopy.

The formation of uridine was confirmed by multidimensional NMR spectroscopy (600 MHz, Bruker). In the correlation spectroscopy (COSY) spectrum, characteristic cross-peaks defined the ribose proton spin system, consistent with a furanose sugar framework (*SI Appendix*, Fig. S3*A*). The heteronuclear single quantum coherence (HSQC) spectrum exhibited well-resolved one-bond correlations, notably the H-1′/C-1′ cross-peak at δH 5.82 to 5.88 ppm/δC 85 to 89 ppm, supporting the assignment of the anomeric ribose carbon (*SI Appendix*, Fig. S3*B*). Importantly, the heteronuclear multiple bond correlation (HMBC) spectrum showed key long-range correlations from H-1′ (δH ~5.8 ppm) to uracil carbons at δC 150 to 153 ppm (C-2), and 140 to 144 ppm (C-6), providing important evidence for N-glycosidic bond formation. In addition, correlations between the aromatic proton H-6 (δH 7.5 to 8.0 ppm) and the uracil carbonyl carbon C-4 (δC 162 to 165 ppm) further supported the structural integrity of the uracil moiety (Fig. 3*E*). Collectively, these diagnostic COSY, HSQC, and HMBC correlations, together

with the characteristic anomeric proton signal, consistently support the successful formation of uridine. Together, these NMR data provide strong structural support for enzyme-free uridine formation in micro- and nanoscale compartments.

Ribonucleoside Formation in Structurally Confined Liposomal Microenvironments.

Liposomes were prepared from nontoxic soybean lecithin by sonication, yielding uniform nanoscale vesicles (17). Cryogenic transmission electron microscopy confirmed well-defined, single-bilayer spherical structures (Fig. 4*A*). Liposomes were loaded with reactants, including nucleobases (adenine, cytosine, hypoxanthine, and uracil), D-ribose, and phosphoric acid. Encapsulation of hypoxanthine and D-ribose was verified by thin-layer chromatography and mass spectrometry, with encapsulation efficiencies of approximately 78 to 79% (*SI Appendix*, Fig. S1 *B*–*E*). Liposomes remained intact in the presence of 697.5 μM phosphoric acid (pH ≈ 4.5), indicating stability under the reaction conditions.

Fig. 4.

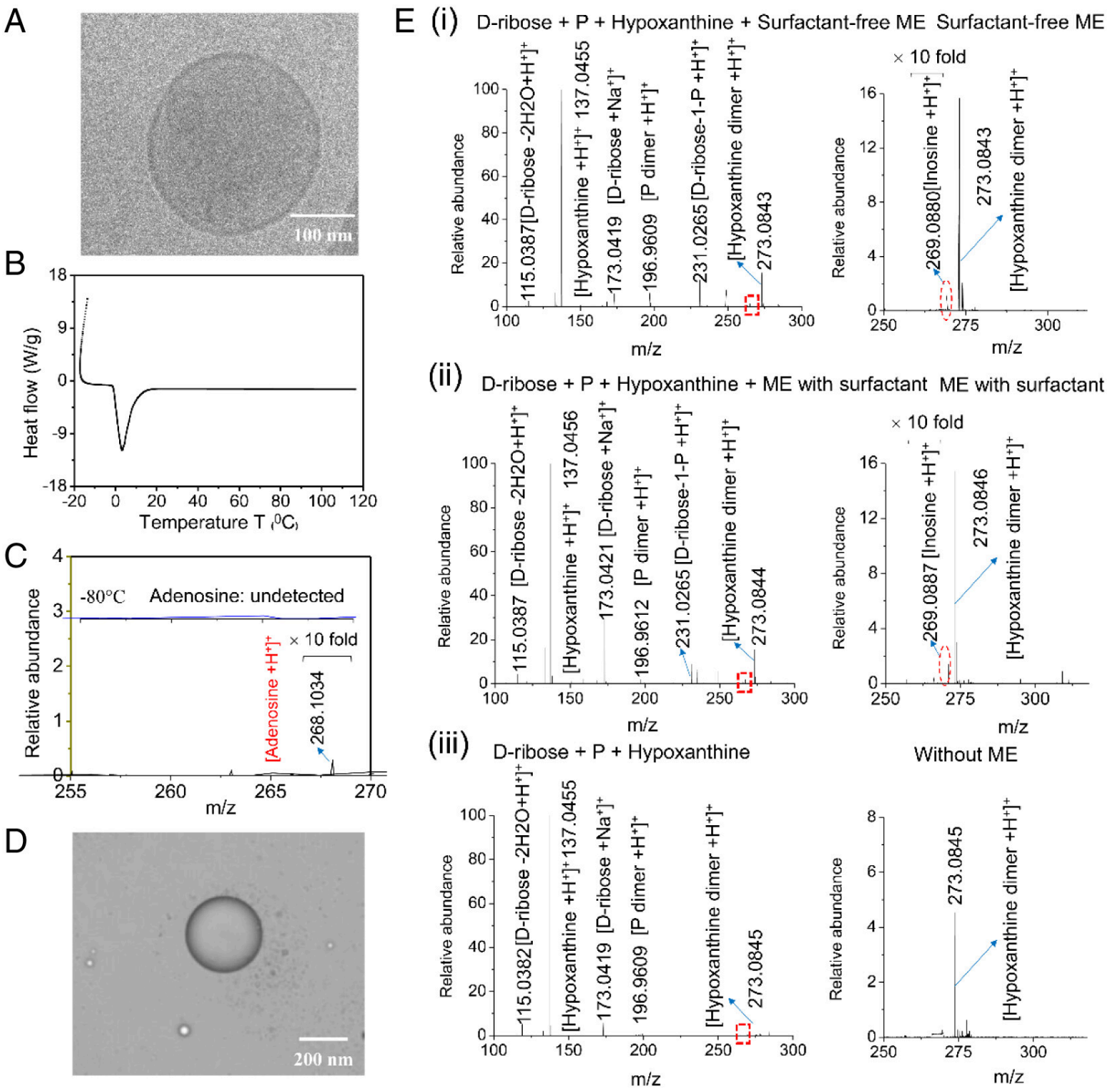

Ribonucleoside formation in liposomal and ME interfacial microenvironments. (A) Cryo-TEM image of liposomes. (B) Differential scanning calorimetry (DSC) trace of the liposomal suspension. (C) ESI-MS spectrum showing adenosine formation in freshly prepared liposomal compartments but not after storage at −80 °C. (D) Optical microscopy image of microemulsions (MEs). (E) Representative ESI-MS spectra of reaction mixtures containing D-ribose, phosphoric acid, and hypoxanthine in (i) surfactant-free MEs, (ii) surfactant-stabilized MEs, and (iii) bulk solution without MEs. Inosine signals were detected selectively in ME systems (red dashed circles).

Following disruption of liposomal membranes using a 1:1 methanol: chloroform mixture, mass spectrometric analysis revealed ribonucleoside formation. Signals corresponding to protonated adenosine [adenosine + H^+]$^+$ (*m/z* 268.1043), inosine [inosine +H^+]$^+$ (*m/z* 269.0882), and uridine [uridine + H^+]$^+$ (*m/z* 245.0770) were detected (*SI Appendix*, Fig. S4 *A–C*). Assignments were supported by accurate mass and CID-MS/MS fragmentation patterns showing diagnostic nucleobase-derived ions (*SI Appendix*, Fig. S5). In addition, phosphorylated ribose intermediates, including [D-ribose-1-phosphate + H^+]$^+$ (*m/z* 231.0261) and [D-ribose + P + H^+]$^+$ (*m/z* 249.0371), were observed. These products were not detected in control experiments conducted in the absence of liposomes, indicating that compartmentalization promoted ribonucleoside formation under nonenzymatic conditions. Cytidine was not detected, indicating nucleobase-dependent product formation under these conditions.

Differential scanning calorimetry (DSC) analysis showed temperature-dependent heat-flow changes, including a transition near −13 °C, consistent with thermally responsive lipid membranes and associated interfacial water environments (Fig. 4*B*). After storage at −80 °C, adenosine formation was no longer observed (Fig. 4*C*), indicating that confinement alone was insufficient when membrane dynamics and interfacial exchange were reduced. Together, these results show that liposomal compartments provide active, membrane-bounded aqueous microenvironments that promote enzyme-free ribonucleoside formation under ambient conditions.

Concentration-Dependent Ribonucleoside Formation in Liposomal Microenvironments.

To examine how precursor and phospholipid concentrations influence ribonucleoside formation within liposomal microenvironments, the concentrations of nucleobases, D-ribose, and liposome-forming phospholipids were systematically varied. In this context, using a liposome suspension diluted from the 4 mM stock to a final phospholipid concentration of 40 μM, increasing hypoxanthine concentration led to enhanced inosine formation, reaching a maximum relative signal intensity of approximately 0.055% at 234 μM hypoxanthine (*SI Appendix*, Fig. S6*A*). A similar trend was observed upon increasing D-ribose concentration from 697.5 μM to 837 μM, with higher D-ribose concentrations yielding increased inosine signals (*SI Appendix*, Fig. S6*B*). For consistency with other experiments, a D-ribose concentration of 697.5 μM was used in subsequent studies.

The effect of phospholipid concentration used for liposome preparation on ribonucleoside formation was then evaluated. The ratios of ribonucleoside ion signals to their corresponding nucleobases exhibited a pronounced dependence on phospholipid concentration, with maximal values observed at 40 μM compared with 10, 20, 80, and 120 μM. At this concentration, adenosine formation reached its highest relative signal, while inosine showed a similar concentration-dependent maximum (*SI Appendix*, Fig. S6 *C*, *i*). Uridine formation also peaked at 40 μM phospholipid concentration, although the enhancement was less pronounced than for adenosine and inosine (*SI Appendix*, Fig. S6 *C*, *ii*).

Collectively, these results indicate that ribonucleoside formation in liposomal systems does not scale monotonically with either precursor concentration or phospholipid concentration. Instead, an intermediate phospholipid concentration provides particularly favorable conditions for nucleoside emergence, consistent with a balance between reactant availability and the number of confined interfacial microenvironments.

It is evident in *SI Appendix*, Fig. S6 that there exists an optimum size of the compartment for nucleoside formation. At first, this finding may seem surprising, but it is consistent with studies reported previously in reference 12. As the radius of a spherical container shrinks, the electric field at the interface strengthens, causing the formation of more radicals. The presence of the radicals drives the reaction to produce products, and this is expected to increase linearly with radical concentration. However, radical–radical recombination also occurs, whose rate is quadratic in the radical concentration. As a consequence of the competition between these two reactions, there is an optimum size of the container to produce reaction products from the reactants (12).

Oil–Water Emulsion Systems Promote Ribonucleoside Formation.

We next asked whether ribonucleoside formation could occur in a third compartment based on spatially distributed oil–water interfaces in microemulsion droplets (17). To this end, two microemulsion (ME) architectures were examined: surfactant-free silicone oil/ethanol ME and a surfactant-stabilized system in which amphiphilic surfactants stabilize the oil–water interface. Optical microscopy confirmed droplet-like morphologies without macroscopic phase separation (Fig. 4*D*).

Dynamic light scattering revealed distinct size characteristics between the two ME architectures, with surfactant-free MEs exhibiting larger domains (~327 nm) and surfactant-stabilized MEs forming smaller, more monodisperse nanodomains (~10.1 nm) (*SI Appendix*, Fig. S6 *D* and *E*). Despite these structural differences, both ME systems supported ribonucleoside formation, indicating that surfactant stabilization is not a prerequisite for reactivity within ME microenvironments.

ME reaction mixtures containing D-ribose (11.25 mM), phosphoric acid (11.25 mM), and nucleobases (3.75 mM) were generated by dilution with purified water (1:100, v/v). Following removal of residual oil components to minimize analytical interference (*SI Appendix*, Fig. S5 *D* and *E*), mass spectrometric analysis revealed reaction products that emerged selectively under ME conditions. In both surfactant-free and surfactant-stabilized MEs (Fig. 4 *E*, i and ii), ion signals corresponding to phosphorylated ribose intermediates [D-ribose-1-phosphate $+H^+]^+$ (*m/z* 231.0261) and inosine [inosine + $H^+]^+$ (*m/z* 269.0880) were detected, whereas these species were absent in bulk solutions lacking MEs (Fig. 4 *E*, iii). Surfactant-free MEs further yielded adenosine, inosine, cytidine, and uridine (*SI Appendix*, Fig. S7), indicating that oil–water ME microenvironments can promote ribonucleoside formation independently of surfactant stabilization.

Mg^{2+} Modulates Ribonucleoside Formation in an Architecture-Dependent Manner.

We next examined how Mg^{2+} modulates ribonucleoside formation across different interfacial compartment architectures, including G/O/W micro/nanobubbles, liposomes, and ME systems. In G/O/W micro/nanobubbles, Mg^{2+} enhanced inosine formation relative to Mg^{2+}-free or oil-only conditions (*SI Appendix*, Fig. S8 *A* and *B*). Adenosine showed a stricter requirement for coupled Mg^{2+} and oil-derived interfaces and was detectable only when both were present (*SI Appendix*, Fig. S8 *C* and *D*).

Micro/nanobubbles generated without sonication showed similar architecture-dependent trends. In double-syringe systems, adenosine formation increased with mixing cycles and was enhanced under Mg^{2+}-containing conditions (*SI Appendix*, Fig. S8*E*). Air-stone experiments further showed that adenosine formation in N_2, CO_2, or air bubbles required Mg^{2+} and/or oil, with no detectable product in their absence (*SI Appendix*, Fig. S8*F*). Cytidine displayed a distinct gas-dependent response: detection required increased cytosine concentration and occurred in CO_2 and air bubbles containing Mg^{2+}, whereas N_2 bubbles remained inactive (*SI Appendix*, Fig. S9). These results indicate that Mg^{2+} effects are nucleoside-specific and depend on gas composition and interfacial architecture.

In liposomes (*SI Appendix*, Fig. S10*A*), we observed nucleoside-specific modulation of product formation when the Mg^{2+} concentration was varied from 140 to 516 μM. Mg^{2+} addition enhanced the permissive response of liposomal microenvironments for adenosine, inosine, and uridine over selected concentration ranges, rather than producing a uniform catalytic effect (*SI Appendix*, Fig. S10*B*). Consistent with this observation, Mg^{2+} may also influence ribonucleoside formation through additional physicochemical effects beyond liposomal microenvironment modulation. Zn^{2+} did not support ribonucleoside formation under comparable conditions, consistent with Zn^{2+}-induced disruption of liposomal integrity and loss of stable compartment-associated microenvironments (18).

In surfactant-free MEs, adenosine was not detected in bulk solution containing Mg^{2+} alone but became detectable after introducing ME compartments (*SI Appendix*, Fig. S11 *A* and *B*). Inosine showed a more permissive response, with detectable signals under selected Mg^{2+}-containing conditions (*SI Appendix*, Fig. S11*C*). Together, these results indicate that Mg^{2+} acts as an architecture-dependent modulator rather than a universal standalone catalyst, altering ribonucleoside formation most consistently in association with structured interfacial microenvironments.

Compartment Size Modulates Ribonucleoside Formation Across Interfacial Architectures.

Having established that bubble size influences ribonucleoside formation in G/O/W micro- and nanobubble systems, we next examined whether size-dependent effects represent a general feature of other interfacial compartment architectures.A similar size dependence was observed in liposomes. Liposomes with diameters ranging from ~200 to ~800 nm were prepared by modulating sonication conditions or by solvent evaporation (*SI Appendix*, Fig. S12

A–C). At a fixed liposome concentration, adenosine, inosine, and uridine formation exhibited nonmonotonic size dependence, with higher relative yield observed for smaller vesicles and reduced formation in larger compartments (*SI Appendix*, Fig. S12*D*). These results indicate that spatial confinement can modulate ribonucleoside formation without introducing new chemical components.

By contrast, ME systems showed limited size sensitivity. Surfactant-free MEs (~320 nm) and surfactant-stabilized MEs (~10 nm) both supported inosine formation with comparable relative signals (Fig. 4*G* and *SI Appendix*, Fig. S12 *E* and *F*). Dye dispersion assays confirmed an oil-in-water ME architecture, suggesting that water-soluble reactants resided mainly in the continuous aqueous phase rather than in droplet interiors (*SI Appendix*, Fig. S12 *G–I*). Consistent with their intrinsic hydrophilicity, D-ribose, phosphate, and nucleobases are therefore unlikely to partition into the oil phase. Thus, in MEs, distributed oil–water interfaces appear sufficient for reactivity, whereas droplet size plays a secondary role. As suggested in the studies reported in references 11 and 12, these results suggest that enhanced reactivity in smaller bubbles and liposomes may be primarily attributed to interfacial curvature, although contributing factors of localized molecular organization may also be present. Together, these results show that size effects are architecture-dependent: smaller bubbles and liposomes enhance reaction permissiveness, whereas ME reactivity is less sensitive to droplet size when reactants are not strongly confined.

Interfacial Microenvironments as a Physical Framework for Ribonucleoside Emergence.

Across the different compartment architectures examined here, ribonucleoside formation was most consistently associated with structured interfacial microenvironments rather than with any single additive, catalyst, or compartment type. Gas–oil–water or gas–water micro/nanobubbles, liposomal vesicles, and ME systems differ substantially in composition and structure, yet each supported ribonucleoside formation under conditions that create confined or interface-rich aqueous regions. This convergence suggests that interfacial organization provides a unifying physical framework for abiotic ribonucleoside formation.

A key insight arising from these results is that interface topology, rather than compartment identity, governs reaction permissiveness. Dual-interface systems such as G/O/W micro/nanobubbles and liposomes couple distinct phase boundaries within a single compartment, whereas microemulsions present spatially distributed single oil–water interfaces. Despite these differences, both topologies support ribonucleoside formation, indicating that the critical requirement is the creation of physically structured aqueous regions adjacent to interfaces. Variations in topology primarily modulate efficiency, stability, and sensitivity to external parameters, rather than determining whether reactions can occur or not. Interfacial environments, such as liquid–air interfaces, have been recognized as important regulators of chemical reactivity in various systems. Our results further suggest that liquid–liquid interfaces can also promote abiotic nucleoside formation by providing structured

microenvironments, indicating that interfacial effects may depend more on local physicochemical properties than interface type alone.

Within this framework, Mg^{2+}, oil phases, surfactants, gas composition, and size act as architecture-dependent modulators. Mg^{2+} altered product formation in a nucleoside- and compartment-dependent manner rather than behaving as a universal standalone catalyst. Oil phases and surfactants influenced interfacial stability and size distributions, but reactivity was also observed in surfactant-free systems. These observations indicate that interfacial microenvironments relax the constraints of homogeneous solution chemistry by creating permissive reaction spaces, within which multiple physicochemical parameters can be tuned without invoking new reaction pathways.

Compartment size further refines this physical framework. In gas-filled bubbles and liposomes, smaller compartments generally enhanced ribonucleoside formation, consistent with stronger confinement and increased curvature (11, 12) but only to some optimum value as shown in *SI Appendix*, Fig. S6. In contrast, in ME systems where reactants reside primarily in the continuous aqueous phase, droplet size exerted a weaker influence on reaction outcomes. This architecture-dependent size effect underscores that confinement and interfacial accessibility collectively define the effectiveness of a given microenvironment.

At the molecular level, the enhanced reactivity within compartmented microenvironments may result from compartment-induced regulation of molecular organization and solvent properties as well as the production of radicals such as H and OH from the charge transfer reaction $H^+ + OH^- \rightarrow H + OH$, in which this process is facilitated by the lack of three-dimensional solvation of H^+ and OH^- and the existence of a strong electric field at the interface. In our system, the gas–oil–water interface within micro- and nanobubble compartments may facilitate favorable interactions among ribose, nucleobases, and phosphate species. Compared with bulk water, nanoscale compartment can promote reactant proximity and orientation, while interfacial hydration structures and hydrogen-bonding dynamics may further create favorable conditions for nucleoside formation. Together, these findings support a physical framework in which micro- and nanoscale interfacial environments, rather than a single catalyst or pathway, expand the conditions under which ribonucleoside formation can occur. By linking G/O/W or G/W bubbles, liposomes, and microemulsions through a common principle of interfacial organization, this work suggests that diverse prebiotic interfaces could have provided permissive reaction spaces for the formation of RNA building blocks.

Conclusion

Taken together, these results show that micro- and nanoscale interfacial compartments can promote the abiotic formation of ribonucleosides from D-ribose, phosphoric acid, and nucleobases under ambient conditions and without enzymatic catalysis. The effect is not restricted to a single compartment type. Gas–oil–water micro/nanobubbles, gas–water micro/nanobubbles, liposomal vesicles, and oil–water microemulsions each provide reaction-permissive environments, although their efficiencies and product distributions differ. This

convergence suggests that interfacial organization, rather than a specific chemical additive or compartment architecture, is the central physical principle enabling ribonucleoside emergence.

Several features of these systems appear especially important. Coupled gas–liquid and liquid–liquid interfaces can enrich reactants, alter local water structure, and create physicochemical conditions distinct from bulk aqueous solution. Compartment size, interfacial curvature, gas composition, oil phase, and Mg^{2+} content further modulate product formation in a nucleoside- and architecture-dependent manner. These findings support the view that early-Earth heterogeneous environments could have offered many small, transient, interface-rich reaction spaces in which otherwise unfavorable prebiotic reactions became more accessible.

This study does not resolve all questions surrounding RNA emergence. The prebiotic sources of activated phosphate, the origin of ribose chirality, the selectivity of N-glycosidic bond formation, and the subsequent conversion of ribonucleosides into polymers remain open challenges. Nevertheless, the present results identify compartmentalized interfacial microenvironments as plausible and broadly available physical settings for the formation and stabilization of RNA building blocks. They therefore add an important environmental dimension to prebiotic chemistry: life's molecular precursors may have emerged not only from different reaction pathways, but also from the micro- and nanoscale interfaces in which those pathways occurred.

Data, Materials, and Software Availability

Study data are included in the article and/or *SI Appendix*.

Acknowledgments

We are grateful to Vijayalakshmi Kanchustambham and Xinwen Xu for their support with cryoelectron microscopy, mass spectrometry, and nitrogen supply. The authors greatly appreciate the support from the Fundamental Research Funds for Central Universities. R.N.Z. thanks the Air Force Office of Scientific Research through the Multidisciplinary University Research Initiative program (AFOSR FA9550-21-1-0170).

Author contributions: Q.L., J.K.L., and R.N.Z. designed research; Q.L. and X.Z. performed research; Q.L., J.K.L., and R.N.Z. analyzed data; and Q.L., J.K.L., and R.N.Z. wrote the paper.

Competing interests: The authors declare no competing interest.

Supporting Information

Appendix 01 (PDF)

DOWNLOAD 2.15 MB

References

1 D. Whitaker, M. W. Powner, On the aqueous origins of the condensation polymers of life. *Nat. Rev. Chem.* **8**, 817–832 (2024).

Go to reference | View | PubMed | Google Scholar | Open URL STANFORD UNIVERSITY

2 A. Ianeselli et al., Physical non-equilibria for prebiotic nucleic acid chemistry. *Nat. Rev. Phys.* **5**, 185–195 (2023).

See all references | View | Google Scholar | Open URL STANFORD UNIVERSITY

3 B. Seelig, I. A. Chen, Intellectual frameworks to understand complex biochemical systems at the origin of life. *Nat. Chem.* **17**, 11–19 (2025).

SHOW ALL REFERENCES

VIEW FULL TEXT | DOWNLOAD PDF

Further reading in this issue

RESEARCH ARTICLE | OCTOBER 5, 2026

Ancient DNA challenges to admixture narratives: Insights from Notre-Dame Cemetery (1683–1796) in Colonial Montreal, Canada

Diane Martin-Moya, Jean-Christophe Grenier, [...] Isabelle Ribot

RESEARCH ARTICLE | OCTOBER 12, 2026

Multidimensional vulnerabilities of informal settlements in the Urban South

Mingxing Chen, Wenming Song, [...] Xuemei Bai

RESEARCH ARTICLE | OCTOBER 12, 2026

Field experiments predict ecological response to a large-scale epidemic of an anti-keystone pathogen

J. Timothy Wootton, Khashiff Miranda, [...] Catherine A. Pfister

Trending

RESEARCH ARTICLE | JUNE 25, 2025

Generative AI without guardrails can harm learning: Evidence from high school mathematics

While generative AI has been shown to enhance productivity, its influence on learning new skills remains unclear. Our research examines the impact of generative AI, specifically GPT-4, on student learning in math education. Through a...

Hamsa Bastani, Osbert Bastani, [...] Rei Mariman

RESEARCH ARTICLE | NOVEMBER 13, 2003

Channelrhodopsin-2, a directly light-gated cation-selective membrane channel

Microbial-type rhodopsins are found in archaea, prokaryotes, and eukaryotes. Some of them represent membrane ion transport proteins such as bacteriorhodopsin, a light-driven proton pump, or channelrhodopsin-1 (ChR1), a recently…

Georg Nagel, Tanjef Szellas, […] Ernst Bamberg

RESEARCH ARTICLE | MAY 12, 2014 |

Active learning increases student performance in science, engineering, and mathematics

The President's Council of Advisors on Science and Technology has called for a 33% increase in the number of science, technology, engineering, and mathematics (STEM) bachelor's degrees completed per year and recommended adoptio…

Scott Freeman, Sarah L. Eddy, […] Mary Pat Wenderoth

VIEW ALL

Sign up for the
PNAS Highlights newsletter

SUBSCRIBE FOR RESEARCH UPDATES

PNAS Proceedings of the National Academy of Sciences of the United States of America

BROWSE

CURRENT ISSUE

PNAS NEXUS

SPECIAL FEATURES

LIST OF ISSUES

TOPICS, COLLECTIONS, AND ARTICLE TYPES

PNAS IN THE NEWS

FRONT MATTER

JOURNAL CLUB

MULTIMEDIA

PODCASTS

EARLY-CAREER RESEARCHERS

INFORMATION

ABOUT

SUSTAINABLE DEVELOPMENT GOALS

EDITORIAL BOARD

AUTHORS

REVIEWERS

SUBSCRIBERS

LIBRARIANS

PRESS

COZZARELLI PRIZE

PNAS UPDATES

Copyright © 2026 National Academy of Sciences. All rights reserved. | Online ISSN 1091-6490
PNAS is a partner of CHORUS, CLOCKSS, COPE, Crossref, ORCID, and Research4Life.